JOURNAL OF THE AMERICAN COLLEGE OF CARDIOLOGY VOL. 77, NO. 23, 2021

AntimiR-132 Attenuates Myocardial Hypertrophy in an Animal Model of Percutaneous Aortic Constriction

Rabea Hinkel, DVM,[a,b,c,d,e,*] Sandor Batkai, PhD,[f,g,*] Andrea Bähr, DVM,[a,b,c] Tarik Bozoglu, PhD,[a,b,c] Sarah Straub, MD,[a] Tobias Borchert, PhD,[g] Janika Viereck, PhD,[g] Andrea Howe, DVM,[a] Nadja Hornaschewitz, DVM,[a] Lisa Oberberger, DVM,[a] Victoria Jurisch, MD,[a] Rainer Kozlik-Feldmann, MD,[h] Franz Freudenthal, MD,[i] Tilman Ziegler, MD,[a,b] Christian Weber, MD,[b,c] Markus Sperandio, MD,[j] Stefan Engelhardt, MD,[b,k] Karl Ludwig Laugwitz, MD,[a,b] Alessandra Moretti, PhD,[a,b] Nik Klymiuk, PhD,[a,b] Thomas Thum, MD, PhD,[f,g] Christian Kupatt, MD[a,b,c]

ABSTRACT

BACKGROUND Pathological cardiac hypertrophy is a result of afterload-increasing pathologies including untreated hypertension and aortic stenosis. It features progressive adverse cardiac remodeling, myocardial dysfunction, capillary rarefaction, and interstitial fibrosis often leading to heart failure.

OBJECTIVES This study aimed to establish a novel porcine model of pressure-overload–induced heart failure and to determine the effect of inhibition of microribonucleic acid 132 (miR-132) on heart failure development in this model.

METHODS This study developed a novel porcine model of percutaneous aortic constriction by implantation of a percutaneous reduction stent in the thoracic aorta, inducing progressive remodeling at day 56 (d56) after pressure-overload induction. In this study, an antisense oligonucleotide specifically inhibiting miR-132 (antimiR-132), was regionally applied via intracoronary injection at d0 (percutaneous transverse aortic constriction induction) and d28.

RESULTS At d56, antimiR-132 treatment diminished cardiomyocyte cross-sectional area (188.9 ± 2.8 vs. 258.4 ± 9.0 μm^2 in untreated hypertrophic hearts) and improved global cardiac function (ejection fraction 48.9 ± 1.0% vs. 36.1 ± 1.7% in control hearts). Moreover, at d56 antimiR-132-treated hearts displayed less increase of interstitial fibrosis compared with sham-operated hearts (Δsham 1.8 ± 0.5%) than control hearts (Δsham 10.8 ± 0.6%). Of note, cardiac platelet and endothelial cell adhesion molecule 1^+ capillary density was higher in the antimiR-132–treated hearts (647 ± 20 cells/mm^2) compared with in the control group (485 ± 23 cells/mm^2).

CONCLUSIONS The inhibition of miR-132 is a valid strategy in prevention of heart failure progression in hypertrophic heart disease and may be developed as a treatment for heart failure of nonischemic origin.

From the [a]Klinik und Poliklinik für Innere Medizin I, University Clinic rechts der Isar, Technical University of Munich, Munich, Germany; [b]Deutsches Zentrum für Herz-Kreislauf-Forschung (German Center for Cardiovascular Research), partner site Munich Heart Alliance, Munich, Germany; [c]Institute for Cardiovascular Prevention, Ludwig-Maximilians-University Munich, Munich, Germany; [d]Laboratory Animal Science Unit, German Primate Centre, Goettingen, Stiftung Tierärztliche Hochschule Hannover, Hannover, Germany; [e]Deutsches Zentrum für Herz-Kreislauf-Forschung (German Center for Cardiovascular Research), partner site Goettingen, Munich, Germany; [f]Institute of Molecular and Translational Therapeutic Strategies, Hannover Medical School, Hannover, Germany; [g]Cardior Pharmaceuticals GmbH, Hannover, Germany; [h]Department of Pediatric Cardiology, University Clinic Eppendorf, Hamburg, Germany; [i]Products for Medicine, SRL (sociedad de responsibilidat limitada), Obajes, La Paz, Bolivia; [j]Walter-Brendel Centre of Experimental Medicine, Ludwig-Maximilians-University Munich, Munich, Germany; and the [k]Institut für Pharmakologie und Toxikologie, Technical University of Munich, Munich, Germany. *Drs. Hinkel and Batkai contributed equally to this work.

The authors attest they are in compliance with human studies committees and animal welfare regulations of the authors' institutions and Food and Drug Administration guidelines, including patient consent where appropriate. For more information, visit the Author Center.

Manuscript received March 5, 2021; revised manuscript received April 1, 2021, accepted April 9, 2021.

Listen to this manuscript's audio summary by Editor-in-Chief Dr. Valentin Fuster on JACC.org.

ISSN 0735-1097 https://doi.org/10.1016/j.jacc.2021.04.028

ABBREVIATIONS AND ACRONYMS

antimiR-132 = antisense microribonucleic acid 132

d3 = day 3

deTAC = disruption of the stent membrane of transverse aortic constriction

dP/dt_{max} = contraction velocity

dP/dt_{min} = relaxation velocity

LV = left ventricle

LVEDP = left ventricular end-diastolic pressure

miR-132 = microribonucleic acid 132

Nrf2 = nuclear factor, erythroid 2 like 2

pTAC = percutaneous transverse aortic constriction

Hypertrophic heart disease is a progressive, heart failure-prone condition caused by mechanical or genetic causes (1). Mechanically, afterload increases by, for example, systemic hypertension or aortic stenosis enhance left ventricular (LV) wall stress and trigger mechanosensing, resulting in cardiomyocyte growth. Genetically, an array of mutations in the myosin heavy chain (*MYH7*), the myosin binding protein C3 (*MybpC3*), or the giant protein titin (*TTN*), among many others, may cause pathological hypertrophy (1). The clinical burden of manifest hypertrophic heart disease comprises the development of overt heart failure (2), increased risk of arrhythmias (3), and a higher morbidity and mortality (4). In cases when mechanical causes are appropriately addressed by efficient antihypertensive treatment or aortic valve replacement, reversion of hypertrophic remodeling is likely to occur, as long as the structural changes of the interstitium are limited. Otherwise, irreversible changes of pathologic hypertrophy become manifest, such as myocardial fibrosis and capillary rarefaction (5). This instance may be present in patients with heart failure with preserved ejection fraction (6), featuring increased myocardial calcium and inflammation levels as well as reduced capillary density (7,8).

This given pleiotropy of pathologic alterations in pressure-overload hypertrophy fits the therapeutic profile of microribonucleic acids, which are known to act on multiple targets. In genetic and pharmacological in vitro and in vivo models, we previously identified microribonucleic acid-132 (miR-132) to be sufficient to induce cardiac hypertrophy but also "necessary" for pathological hypertrophy in vivo (9), involving a strong effect on cardiomyocyte hypertrophy and calcium signaling. Moreover, a translational pig study in myocardial infraction induced heart failure revealed that the application of antisense microribonucleic acid-132 (antimiR-132) at day 3 (d3) after myocardial infarction followed by a second application at d28 improved systolic function at d56 significantly (10). In a subsequent clinically relevant pig study of chronic ischemia-induced heart failure, followed up for 6 months, an ~8% absolute increase of ejection fraction and a significant improvement of diastolic function was accompanied by antifibrotic and antihypertrophic effects (11). Translating this concept to clinical application, a first-in-class microribonucleic acid inhibitor against miR-132 (CDR132L) for the treatment in heart failure was developed and 28 stable patients with chronic heart failure have been treated with CDR132L in a phase 1b study (Clinical Study to Assess Safety, PK and PD Parameters of CDR132L; NCT04045405), showing safety and potential first efficacy signals such as a more than 20% reduction of N-terminal pro-B-type natriuretic peptide levels in patients treated for heart failure on top of standard-of-care (12).

However, the concept of therapeutic miR-132 inhibition in a large animal model of nonischemic heart failure with cardiac hypertrophy and fibrosis has not been studied yet. Such a model may be of particular interest, because inhibition or deletion of miR-132 derepressed angiogenesis in vitro and in rodents in vivo, respectively (13), potentially preventing the transition of physiologic to pathologic hypertrophy. Here, the contribution of reactive oxygen species to cardiac hypertrophy via the exhaustion of antioxidative defense systems may be amenable to de-repression of miR-132-dependent detoxification signals such as nuclear factor, erythroid 2 like 2 (*Nrf2*). This putative mechanism has been implied in an earlier rat study showing that angiotensin II, a powerful inducer of hypertrophy, up-regulates the miR-212/132 cluster (14). Of note, *Nrf2* is a target of sirtuin 1, a class III histone deacetylase, which is down-regulated by miR-132 (15). Moreover, capillary rarefaction is a critical step from physiologic to pathologic hypertrophy (7), which may be attenuated by de-repressing growth factor receptor-bound protein 1-associated binding protein 1 (*Gab1*), a vasoactive factor with a miR-132 binding site (13).

In the current study, we assessed the role of an intensified myovascular cross talk in a novel preclinical pig model of inducible myocardial hypertrophy, which replicates the clinical picture of LV pressure overload due to aortic stenosis or more broadly hypertension, by percutaneous implantation of a reduction stent into the thoracic aorta (or percutaneous transverse aortic constriction [pTAC]). In this model, we applied antimiR-132 via intracoronary application to inhibit cardiac miR-132 twice, at the time of stent implantation and 4 weeks later. We investigated the cardiac function over time and assessed molecular and histological parameters 8 weeks after implantation.

SEE PAGE 2936

METHODS

Pigs were purchased from the Department of Veterinary Medicine, Ludwig-Maximilians University of Munich (Oberschleißheim, Germany). Animal care and all experimental procedures were performed in

FIGURE 1 Workflow of the Model: Aortic Stent-Induced Cardiac Hypertrophy

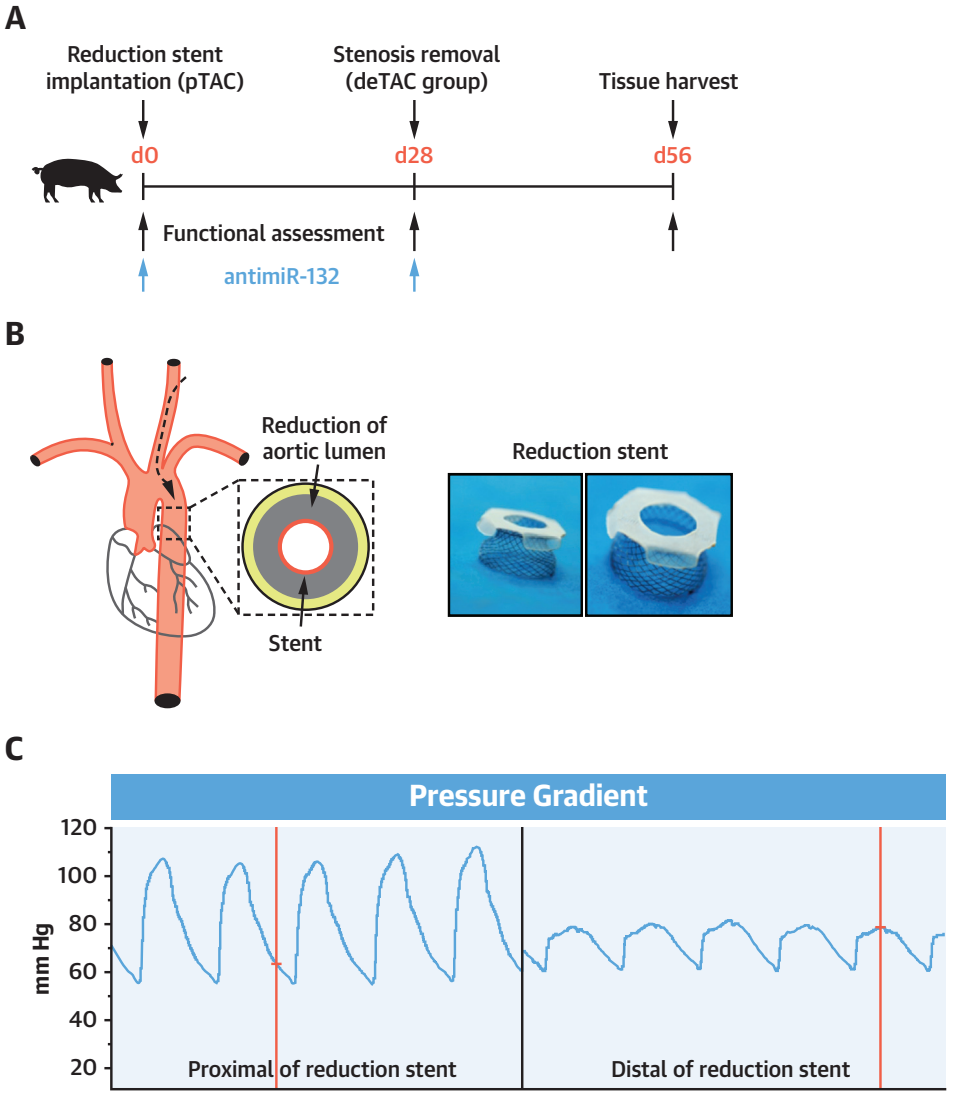

(A) A nitinol-based reduction stent (PFM) **(right panel)** featuring a PTFE (polytetrafluoroethylene) membrane was inserted via the common carotid artery **(left panel),** decreasing the surface area of the descending thoracic aorta by 60% (percutaneous thoracic aortic stent implantation, or percutaneous transverse aortic constriction [pTAC]). **(B)** Experiments were initiated by implantation of the reduction stent at day 0 (d0), accompanied by left ventricular angiography and invasive blood pressure measurements before and after implantation (= functional assessment). At d0 and d28, antisense microribonucleic acid-132 (antimiR-132) was infused into the left coronary arteries (left anterior descending artery, circumflex artery), and the cumulative dose was 0.5 mg/kg. Functional assessment was repeated at d28 and d56, complemented by open-chest subendocardial segment shortening assessment of functional reserve, before the experiment was terminated and tissue was harvested for histologic analyses. **(C)** Invasive pressure tip recordings reveal a pressure difference of about 30 mm Hg between the vessel regions proximal and distal to the reduction stent. This difference could be annihilated by inflation of a 20-mm True Dilatation (BD Interventional Heidelberg, Germany) balloon inside the stent (resulting in disruption of the stent membrane of transverse aortic constriction [deTAC]).

strict accordance to the German and National Institutes of Health animal legislation guidelines and were approved by the Bavarian Animal Care and Use Committee (AZ 55.2-1-54-2532-141-11 and 55.2-1-54-2532-62-13).

PORCINE pTAC STENT MODEL. Pigs (n = 5 for pTAC placebo control, n = 6 for pTAC antimiR-132, n = 7 for sham experimental group) were instrumented at d0. In general anesthesia, a 10-F sheath was retrogradely inserted into the left carotid artery and advanced into

FIGURE 2 Hemodynamic Alterations After Stent Implantation (pTAC) and Removal (deTAC)

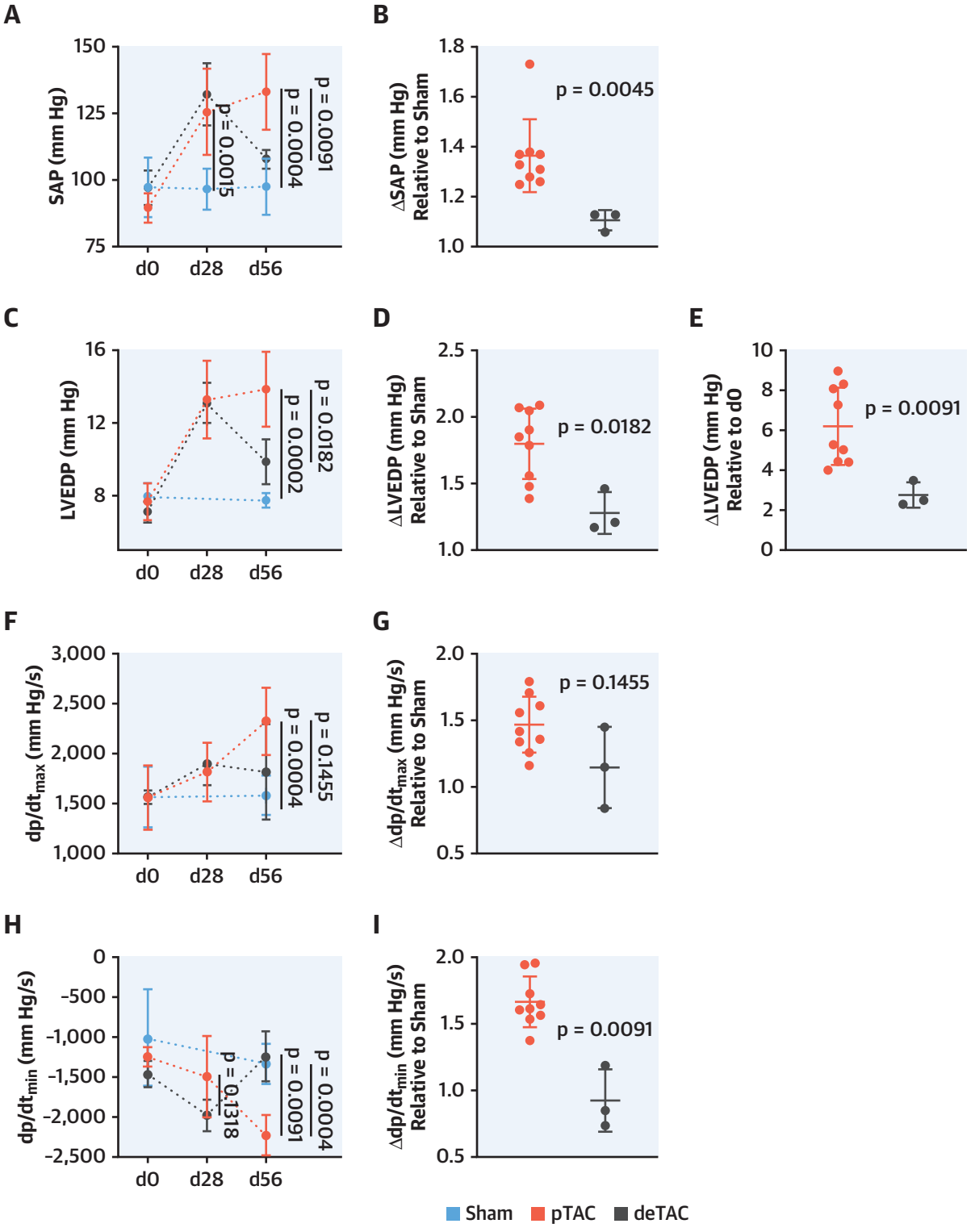

(A and B) Systolic aortic pressure (SAP) in the pTAC group increased until d56, whereas removal of the reduction stent stenosis (= deTAC) decreased the SAP to sham level. **(C to E)** Left ventricular end-diastolic pressure (LVEDP) increased on pTAC until d56, unless deTAC at d28 was followed by a significant decrease. **(F to I)** The contraction velocity (dP/dt_{max}) increased significantly until d56 **(F and G),** except for in the deTAC group, accompanied by an increased relaxation velocity (dP/dt_{min}) **(H and I)**. Abbreviations as in Figure 1.

FIGURE 3 Systolic Cardiac Function After Stent Implantation (pTAC) and Removal (deTAC)

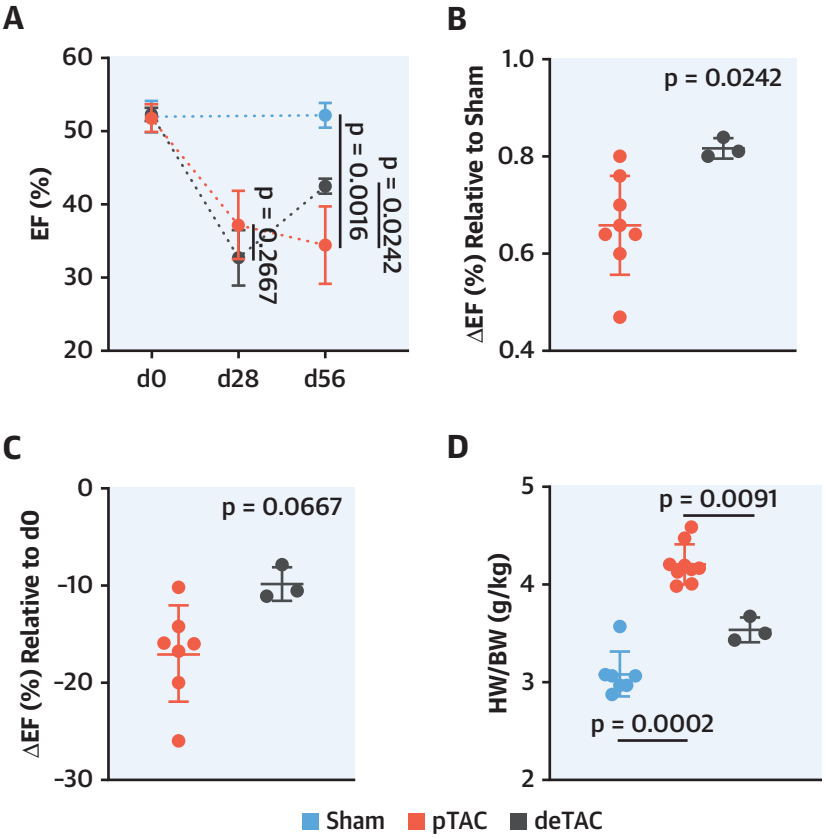

(A to C) Ejection fraction (EF) decreased at d28 and d56 after pTAC and was partially reversed after deTAC at d28. **(D)** Heart weight to body weight (HW/BW) ratios at d56 were significantly increased after pTAC, but statistically were not different from sham level after deTAC. Abbreviations as in Figure 1.

the aorta. Via the sheath, an aortic reduction stent (Figure 1) was inserted into the proximal descending thoracic aorta. After release of the stent, a membrane inside the stent reduced the aortic lumen by 60%, leading to an immediate rise of blood pressure by 12 mm Hg. Over the following 8 weeks, another 25 mm Hg increase of blood pressure was observed (Figure 2A), unless the stent membrane is disrupted (deTAC) by balloon valvuloplasty and the pressure dropped by 10 mm Hg immediately and a total of 20 mm Hg over the following 4 weeks.

REGIONAL antimiR-132 TREATMENT. Recently, we investigated optimal treatment doses in a porcine myocardial infarction model (10). In the current study, we regionally applied antimiR-132 via antegrade application at d0: 10 mg antimiR-132 into the left anterior descending artery and 5 mg into the circumflex artery, each using an over-the-wire balloon (2.5 × 12 mm) inflated at 4 bars for 3 min to slow blood flow into the target region and to increase contact time for the drug infusion. An identical application was repeated at d28, using the same regional approach (Figure 1A).

In total, 1 animal of the control group was lost during anesthesia due to an underlying lung disease, whereas all treated animals survived and were included in the study.

HEMODYNAMIC MEASUREMENTS. Invasive monitoring of aortic pressure as well as LV function was obtained using a standard pressure tip catheter percutaneously introduced into the aorta and the LV lumen (ADV500, Transonic, Ithaca, New York) under fluoroscopic control of the correct positioning for the measurements. Systolic aortic pressure and left ventricular end-diastolic pressure (LVEDP) measurements were made before pTAC, as well as at d28 and d56 after stent implantation. Contraction velocity (dP/dt_{max}), and relaxation velocity (dP/dt_{min}) were

FIGURE 4 Hemodynamic Alterations After Stent Implantation Are Attenuated by AntimiR-132

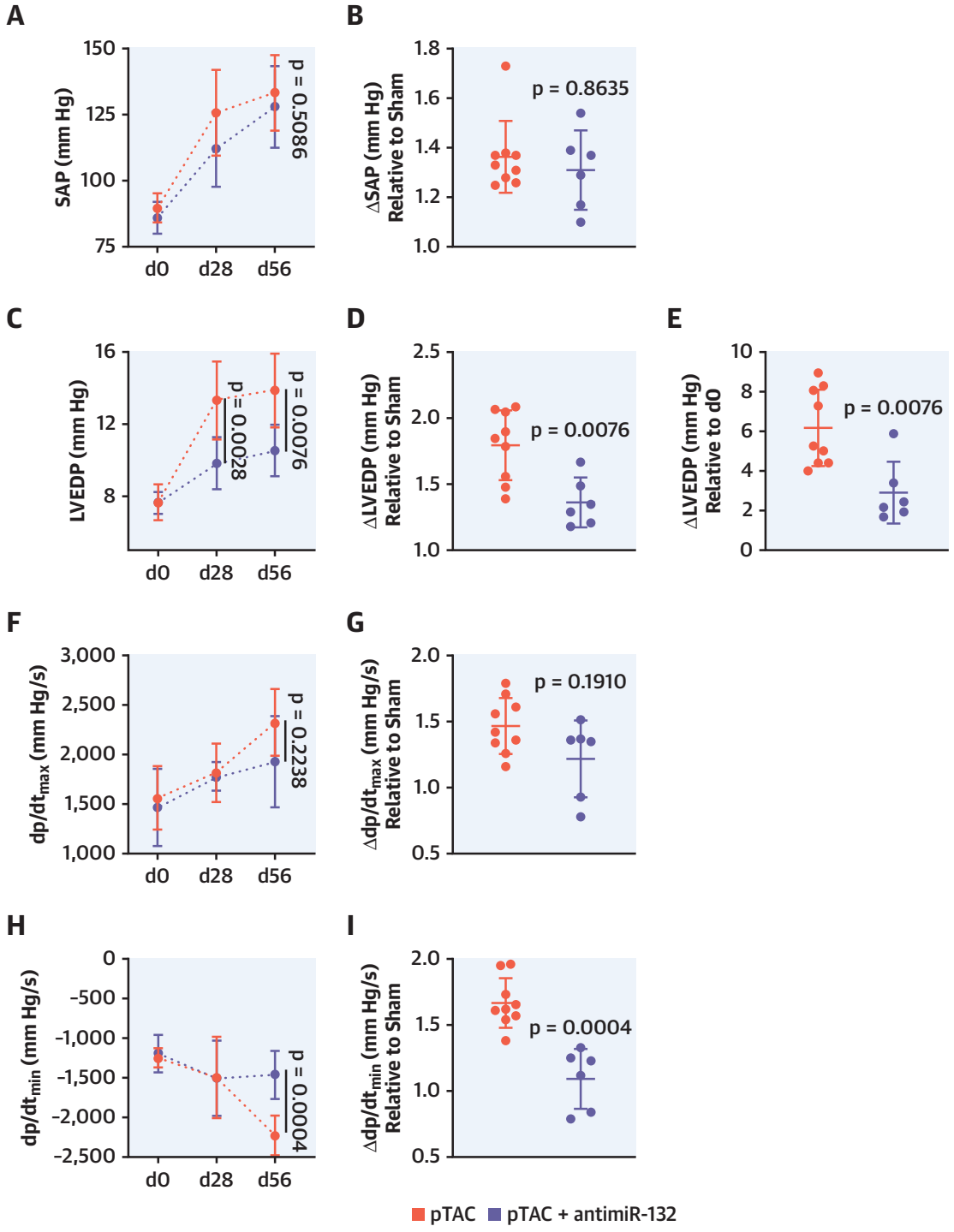

(A and B) SAP increased analogously in pTAC pigs with or without antimiR-132 treatment (0.5 mg/kg intracoronary) (Methods), with no difference relative to sham-operated animals. **(C to E)** LVEDP increase was attenuated after antimiR-132 treatment. **(F to I)** Whereas no significant alteration of dP/dt_{max} was found after antimiR-132 treatment **(F and G),** and dP/dt_{min} was maintained at levels indistinguishable from that of sham animals **(H and I)**. Abbreviations as in Figures 1 and 2.

FIGURE 5 AntimiR-132 Reduces Systolic Heart Failure in Hypertrophic Hearts

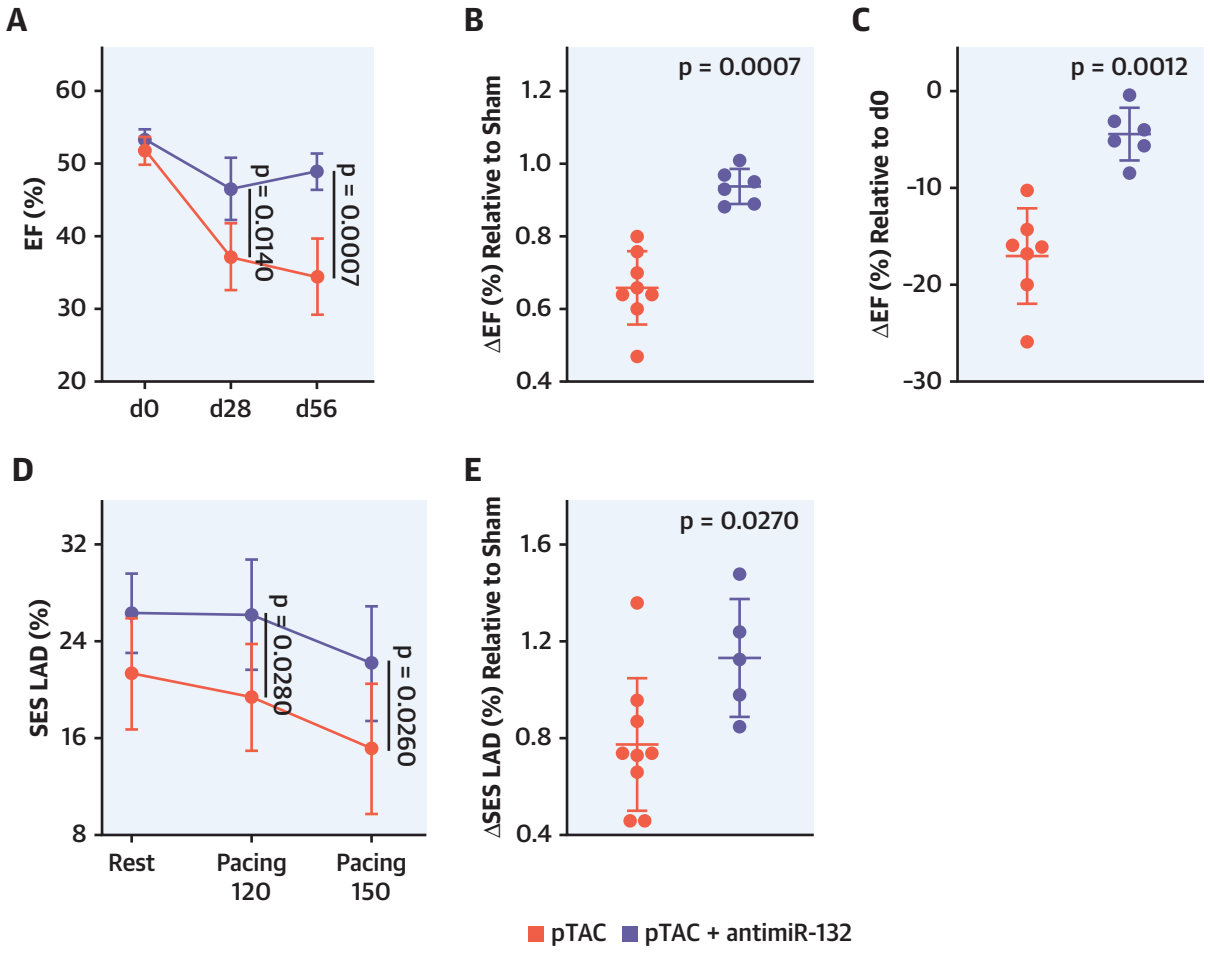

(A to C) Systolic function, assessed as EF was preserved after antimiR-132 treatment until d56, as opposed to in untreated control animals. **(D and E)** Subendocardial segment (SES) shortening declined over time after pTAC and was significantly improved after antimiR-132 application. LAD = left anterior descending; other abbreviations as in Figures 1 and 3.

determined under resting heart rate as well as atrial pacing at 120 and 150 beats/min (for 1 min each).

MICROVASCULAR DENSITY. For pig immunofluorescence, heart samples were frozen on dry ice, embedded in optical cutting temperature compound, and sectioned onto slides. Heart slides were fixed in cold acetone, washed in phosphate-buffered saline (5 min, 3 washes), and blocked with 10% normal fetal serum (NFS), for 60 min. Then, slides were incubated overnight at 4°C with the following antibodies (diluted in blocking buffer): Anti PECAM-1 (sc-376764, 1:50; Santa Cruz Biotechnology, Dallas, Texas), anti NG2 (NG2 antibody, AB5320, 1:200; Millipore Corp., Bedford, Massachusetts). The slides were washed with phosphate-buffered saline (5 min, 3 washes) and stained with the relevant secondary antibody for 2 h at room temperature. Slides were mounted and visualized.

CARDIOMYOCYTE SIZE. To determine the cross-sectional area of cardiomyocytes, 8-μm thick cardiac sections were stained with Alexa Fluor 647-conjugated wheat germ agglutinin (Life Technologies, Thermo Fisher Scientific, Waltham, Massachusetts) and embedded with a 4′,6-diamidino-2-phenylindole-containing vecta shield (Life Technologies) (16). Images were acquired with a 20× objective using Leica Thunder microscope (Leica, Hilden, Germany) and Image J software (National Institutes of Health, Bethesda, Maryland) was applied to determine the average cross-sectional area of cardiomyocytes in 1 section (>50 cells per section; 300 to 500 cells per heart).

FIGURE 6 **AntimiR-132 Regulates Cardiac Fibrosis, Cardiomyocyte Size, and Microvascularization In Vivo**

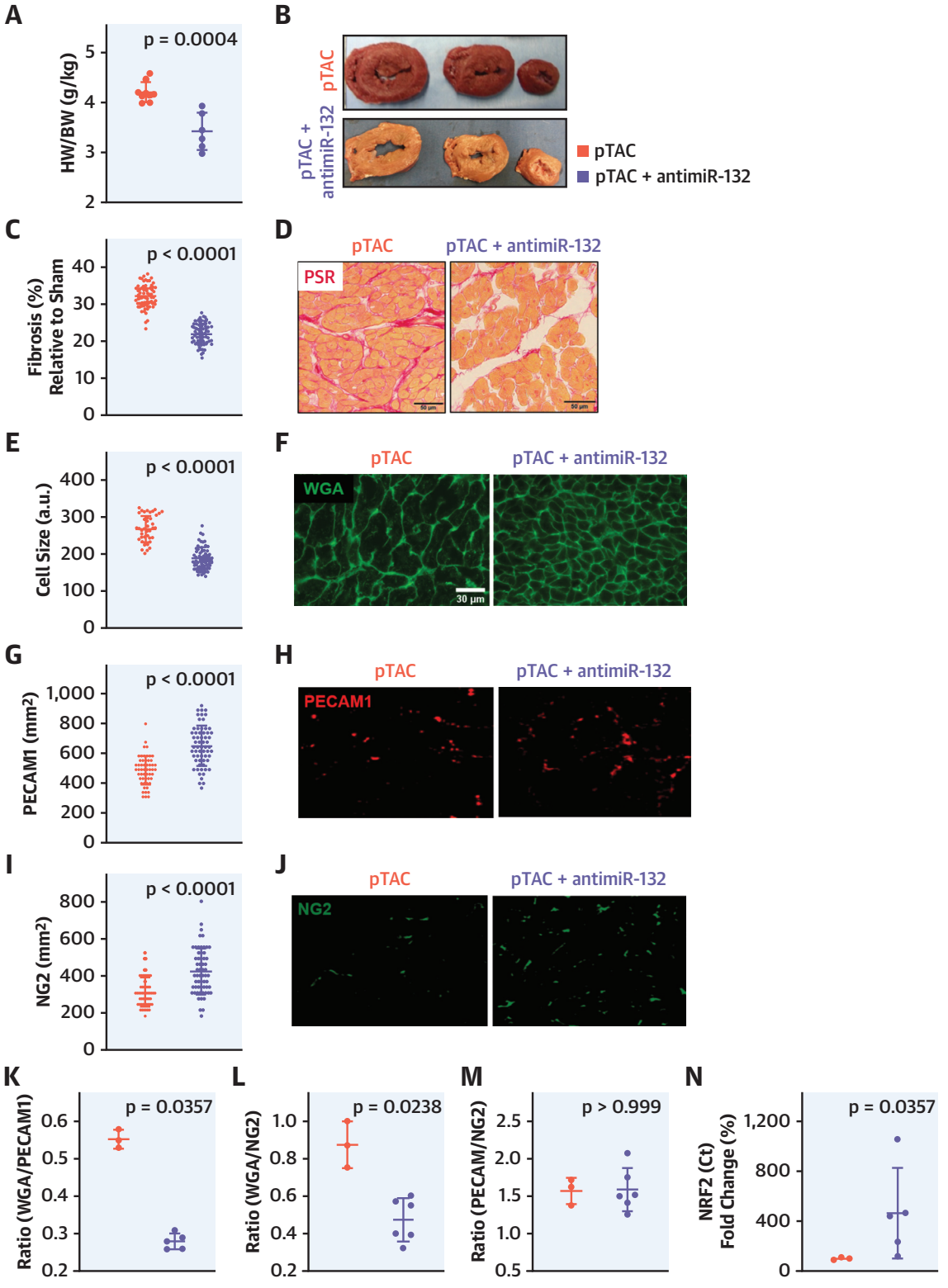

Continued on the next page

FIBROSIS STAINING. Cryosections (8 μm) were generated using standard histological techniques. For quantification of collagen deposition, myocardial sections were stained with sirius red and fast green. Images were acquired using a Leica Thunder microscope with a 10× objective and fibrosis was quantified using Image J software.

QUANTITATIVE REAL-TIME POLYMERASE CHAIN REACTION. Total ribonucleic acid was extracted from tissue using and reverse-transcribed into complementary deoxyribonucleic acid. Quantitative real-time polymerase chain reaction was performed on an iQ-cycler (Bio-Rad, Munich, Germany) with SYBR-Green Supermix (Bio-Rad). For quantitative polymerase chain reaction, the following primers were used: glyceraldehyde 3-phosphate dehydrogenase (*GAPDH*) forward: 5′-AATTCAACGGCACAGTCAAG-3′, reverse 5′-ATGGTGGT-GAAGACACCAGT-3′; *NRF2* forward: 5′-GGGGTAAGAATAAAGTGGCTGCTC-3′, reverse: 5′-ACATTGCCATCTCTTGTTTGCTG-3′.

STATISTICAL ANALYSIS. The results are given as mean ± SD. Statistical analysis of results between >2 experimental groups was performed with 1-way analysis of variance. Whenever a significant effect was obtained with analysis of variance, we performed multiple comparison tests between the groups using the Mann-Whitney *U* test. Two experimental groups were compared by Student's *t*-test. Differences between groups were considered significant at $p < 0.05$. All procedures were performed with an SPSS statistical program version 25 (IBM Corp., Armonk, New York).

RESULTS

First, we sought to establish a realistic and clinically relevant hypertrophy model in porcine hearts by percutaneous means, to avoid excessive animal loss and potential confounding factors of a large thoracotomy wound. Therefore, we developed a membrane-carrying nitinol stent (Products for Medicine, La Paz, Bolivia), which was advanced via the left carotid artery into the descending thoracic aorta and released under fluoroscopic control just distal to the ostium of the left subclavian artery. This maneuver sufficed to reduce the cross-sectional area of the descending thoracic aorta to 40% of the original diameter at d0 (pTAC) (**Figures 1A to 1C,** Supplemental Figures 1A and 1B). An increase of LV pressure from 89.7 ± 2.4 mm Hg to 101.4 ± 2.3 mm Hg ($p < 0.05$) was observed immediately, with no differences between experimental groups. Without further intervention, a second increase of systolic LV pressure to 129.7 ± 2.1 mm Hg ($p < 0.005$) occurred in the pTAC group (**Figure 2A,** Supplemental Figures 1A and 1B), unless the stent membrane was disrupted with a balloon (deTAC group) at d28 and the systolic pressure dropped in the deTAC group from 126.3 mm Hg to 105.5 ± 2.0 mm Hg ($p < 0.01$) (**Figures 1C and 2A,** Supplemental Figures 1A and 1B). Aortic pressure and maximal LV pressure were proportional over the whole experimental timeline ($r = 0.845$, $p < 0.001$) (Supplemental Figure 1C), underscoring increased LV filling pressure depending on peripheral aortic resistance. Of note, the LVEDP increased significantly compared with sham, unless deTAC was applied (**Figures 2C to 2E,** Supplemental Figures 2A to 2D). Both, dP/dt_{max} as well as dP/dt_{min} increased with increasing pressure (**Figures 2F to 2I**). Despite these compensatory mechanisms, the ejection fraction of pTAC hearts deteriorated from 52.0 ± 2.0% to 34.5 ± 2.0%, unless deTAC allowed for partial restoration (43.8 ± 0.5%) (**Figures 3A to 3C,** Supplemental Figures 2A to 2F). The rise in afterload under pTAC conditions increased heart weight to body weight ratio from 3.1 ± 0.3 g/kg to 4.2 ± 0.3 g/kg, unless deTAC reduced it to 3.6 ± 0.2 g/kg (**Figure 3D**).

After establishing the model of pathologic hypertrophy due to pTAC-increased afterload, we assessed whether prevention of the transition from physiologic to pathologic hypertrophy was feasible by inhibition of miR-132, itself a driver of pathologic hypertrophy (17). Therefore, we applied antimiR-132 into coronary arteries at 2 time points, d0 (reduction stent implantation) and d28 (**Figure 1B**). Noteworthily, local application of antimiR-132 (15 mg per animal) did not

FIGURE 6 Continued

(A) The HW/BW (heart weight/body weight) ratios were significantly reduced after pTAC by antimiR-132 treatment. **(B)** This effect concurred with the macroanatomic appearance of examples of hypertrophic cross-sections of pTAC ventricles (**upper panel,** note the almost complete consumption of a ventricular lumen), which was attenuated by antimiR-132 treatment. **(C and D)** Interstitial fibrosis induced by pTAC was attenuated by antimiR-132. Bars = 50 μm. **(E and F)** Compared with pTAC, cardiomyocyte cross-sectional area was significantly diminished by antimiR-132 treatment. Bars = 30 μm. **(G to J)** Capillary density, assessed by PECAM-1 staining of endothelial cells **(G and H),** revealed an increase of microvascular density, with a concomitant increase in NG2+-pericyte density **(I and J),** indicating preservation of a mature microvascularization. **(K to M)** Ratio of wheat germ agglutinin (WGA) to PECAM1, WGA to NG2, and PECAM1 to NG2. **(N)** Expression of *NRF2* at d56.
a.u. = arbitrary units; Ct = cycle threshold; NRF2 = nuclear factor, erythroid 2 like 2; PSR = picro-sirius red.

CENTRAL ILLUSTRATION **Prevention of Myocardial Hypertrophy via AntimiR-132**

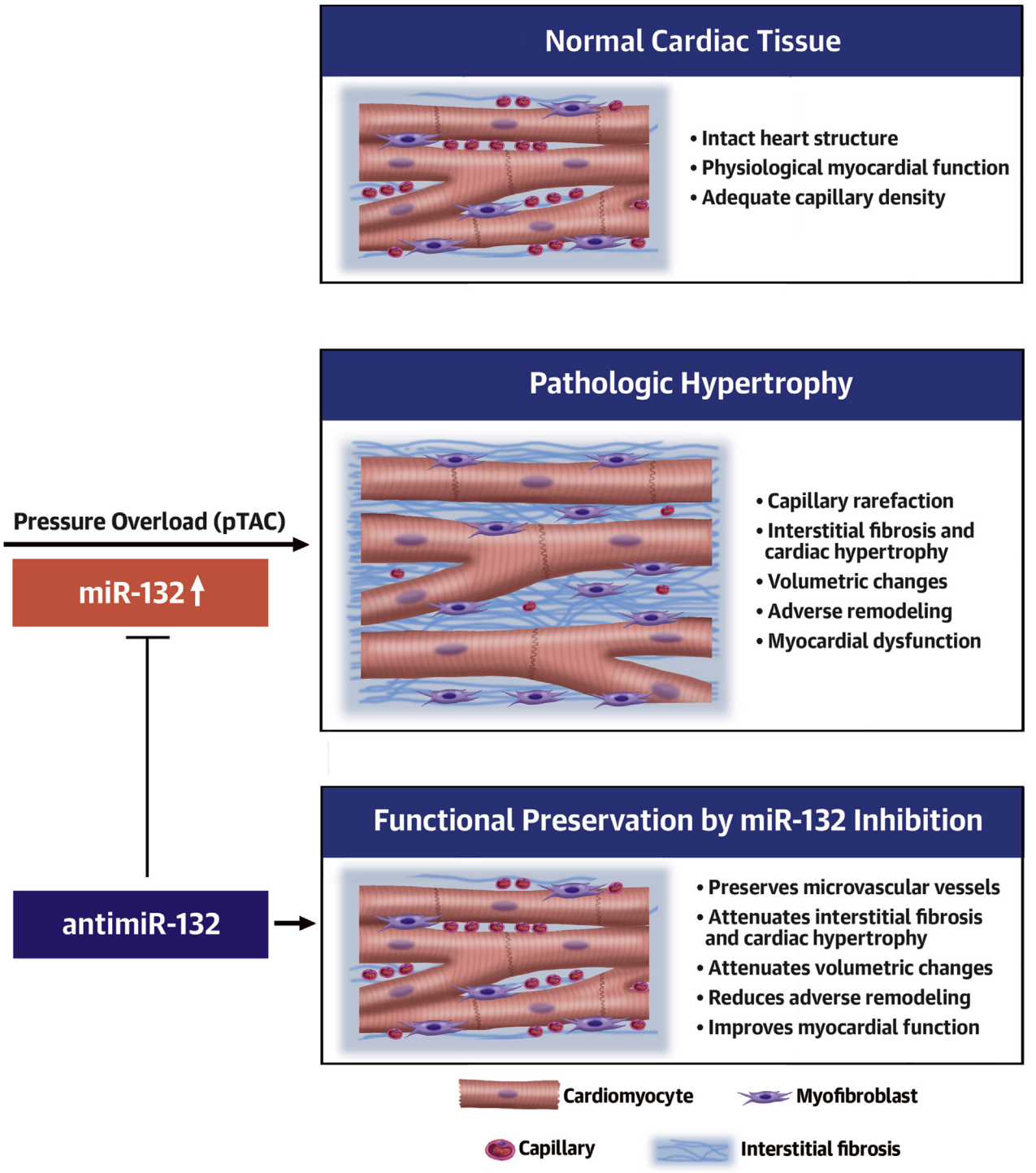

Hinkel, R. et al. J Am Coll Cardiol. 2021;77(23):2923–35.

Pressure-overload hypertrophy, a clinical condition is leading to cardiac failure, has been induced via percutaneous transverse aortic constriction (pTAC) in our preclinical pig model. Whereas control animals developed cardiomyocyte growth leading to a massive hypertrophy on an increased afterload, intracoronary application of antisense microribonucleic acid-132 (antimiR-132) at days 0 and 28 significantly attenuated this effect. Moreover, capillary rarefaction, interstitial fibrosis, and adverse remodeling were blunted, preventing the stigmata of pathologic hypertrophy. Therefore, the inhibition of miR-132 may be developed as a treatment for heart failure of nonischemic, pressure-overload origin. Clinical studies of antimiR-132-therapy in pressure-overload hypertrophy seem warranted. miR-132 = microribonucleic acid-132.

result in a significant decrease in aortic pressure (Figures 4A and 4B) at d28 or d56.

On the other hand, LVEDP, a prognostic marker of heart failure, was found to be less elevated after antimiR-132 treatment in heart failure animals compared with in control animals (Figures 4C and 4E), indicating prevention of the transition from physiologic to pathologic hypertrophy. Contraction and relaxation velocities displayed less increase than did sham control animals, with dP/dt_{min} reaching significance (Figures 4H to 4I). Nevertheless, the LV ejection fraction was preserved at 46.5 ± 1.8% (d28) and 48.9 ± 1.0% (d56), which was significantly different from that of the control group (35.8 ± 2.1% [d28], 36.1 ± 1.7% [d56]) (Figures 5A to 5C). Consistently, the functional reserve assessed as regional myocardial contraction in the anterolateral wall (left anterior descending artery perfusion region) was better preserved (Figures 5D and 5E). In contrast, following antimiR-132 treatment, the heart weight to body weight ratio index decreased (Figures 6A and 6B), indicating reduction of a pathological hypertrophy. A requirement for this effect would be reduced cardiac fibrosis development (compared with that of sham animals). Indeed, the difference in fibrotic area of control pTAC versus sham was 10.8 ± 0.6%, which was found to have reduced to 1.8 ± 0.5% after antimiR-132 treatment (Figures 6C and 6D). This behavior was associated with a less extensive increase of individual cardiomyocyte size, as depicted in Figures 6E and 6F. In contrast, the microcirculatory density of platelet and endothelial cell adhesion molecule 1 (PECAM-1^+) capillaries in the antimiR-132 group (647 ± 20/mm^2) was found higher than in the control group (494 ± 22/mm^2), although not reaching sham values (764 ± 13/mm^2) (Figures 6G, 6H, and 6K). Consistent with a more mature microcirculatory status, pericyte coverage of the microcirculation, assessed by neural/glial antigen 2 (NG2) staining, was found to be higher, reaching sham values (389 ± 11/mm^2), in the antimiR-132 group (420 ± 27/mm^2) than in the control group (311 ± 5/mm^2) (Figures 6I, 6J, 6L, and 6M).

Further investigating the hypertrophy-associated vessel-depriving mechanism dysregulated in cardiomyocytes, we assessed activation of the antioxidant master-regulator *Nrf2* during pTAC. Of note, myocardial tissue exposed to antimiR-132 displayed a higher amount of *Nrf2* than untreated cardiac tissue in pTAC animals, as assessed by quantitative real-time polymerase chain reaction analysis (Figure 6N).

DISCUSSION

In the present study, we demonstrate in a novel porcine preclinical model of percutaneous aortic constriction by stent implantation (pTAC) that antimiR-132 attenuates excessive cardiac hypertrophy coupled with microvascular rarefaction and loss of myocardial function (Central Illustration). In the pTAC model, the increase in blood pressure of about 40 mm Hg over 8 weeks, antimiR-132, applied regionally to the coronary arteries twice with a 4-week interval, did not affect systolic blood pressure, but it preserved ejection fraction, which otherwise deteriorated over time. Analysis of diastolic wall thickness, myocardial cross-sectional area, and heart weight to body weight ratio indicated a massive hypertrophic remodeling after pTAC, which was significantly attenuated by regional antimiR-132 application. Histologically, myocardial fibrosis and microvessel rarefaction were largely prevented by the regional antimiR-132 application.

In this paper, we have developed a percutaneous model of hypertrophy induction by placing a lumen-reducing stent in the descending thoracic aorta. Over 28 days, a pressure increase of 35 to 40 mm Hg was ensured, which was maintained to d56. Interestingly, ejection fraction was depressed, whereas LVEDP was increased at d28, indicating the onset of pathologic hypertrophy in the first 4 weeks of hypertrophy. However, deTAC at d28 shows half-normalization of ejection fraction, heart weight to body weight ratio, dP/dt_{max}, and LVEDP; in addition, dP/dt_{min} and systolic arterial pressure were indistinguishable from sham levels at d56, indicating reversibility of pressure-overload hypertrophy at least up to d28. This model corresponds well to the murine TAC model, displaying pathologic hypertrophy after 14 days of thoracic aortic banding. However, it avoids the surgical part of the mouse model, which may cause inflammation affecting the results of the experiment and may substantially increase dropout risk in a porcine model. Also, this model is more translational, closely mimicking the human clinical situation of aortic stenosis, LV pressure-induced remodeling, and heart failure.

In antimiR-132 treated pTAC hearts, ribonucleic acid analysis revealed an increase of *Nrf2* in porcine myocardium compared with in untreated pTAC control hearts at the 8-week time point (Figure 6N), indicating an improved antioxidant response in the antimiR-132–treated tissue. These data are consistent with earlier findings of a down-regulation of *Nrf2* by miR-132 repressing sirtuin-1 in vitro (18), which has previously been shown to prevent expression of the vasoactive factor sirtuin-1 in vitro (13).

Our model of porcine pTAC, as well as murine TAC, provides the hallmark of pressure-induced pathologic hypertrophy, namely capillary rarefaction (Figure 6) (7). It is well-known that

vascularization, rather than sheer ventricular mass or volume, determines function in pressure-overload hypertrophy, such that pathologic hypertrophy was avoided in mice undergoing forced hypervascularization (19).

However, usually pressure-induced hypertrophy transits from the physiologic to the pathologic phenotype, at least in part due capillary rarefaction. One reason for this loss of microcirculatory networks may consist of insufficient proangiogenic signaling in pressure-challenged cardiomyocytes (20), paired with an up-regulation of angiostatic thrombospondin-1 or vessel-destabilizing angiopoietin-2 (21). Second, macrophage proliferation and monocyte recruitment induce low-level inflammation in the mechanically stressed myocardium, for example, 8 weeks after myocardial infarction (22) or in angiotensin II-induced cardiac hypertrophy (23), and are associated with capillary rarefaction in angiotensin II-induced hypertension (24). Third, replacement fibrosis of cardiomyocytes, described in diabetic cardiomyopathy (25), could cause capillary rarefaction in cardiac hypertrophy. Mechanistically, nicotinamide adenine dinucleotide phosphate oxidases (*Nox2*, *Nox4*) play a role in angiotensin II- and TAC-induced hypertrophy (26), generating reactive oxygen species such as H_2O_2, which induces expression of the miR-212/132 cluster in H9C2 cardiomyocytes (27). On the other hand, *Nrf2*, a master regulator of antioxidant defense genes, attenuates TAC-induced hypertrophy (28). Expression of *Nrf2* was found increased by antimiR-132 in vitro (**Figure 6**), in addition to the well-known miR-132 targets *FoxO3* and sirtuin 1 (9,13). Within the capacity of sirtuin 1de-repression (29), antimiR-132 treatment induced a higher density of capillaries, but also pericytes in vivo (**Figure 6**), indicating the involvement of capillary growth and maturation factors (30,31) in the preservation of physiologic hypertrophy. These findings fit the notion that antimiR-132 application affects both the cardiomyocyte and endothelial compartments in vitro and in vivo (9,13), potentially inducing growth in endothelial cells and modulating cardiomyocyte behavior toward angiogenesis induction.

STUDY LIMITATIONS. For this study, we deliberately chose a local inhibition of a low dose of miR-132 to modify the continuous stimulus of pTAC. We achieved the prevention of a pathologic hypertrophic state by applying antimiR-132 twice into coronary arteries, similar to a monthly administration of antimiR-132 in a different (chronic ischemic) heart failure model (11). Whether a similar effect may be accomplished by intravenous application of a higher dose of antimiR-132 requires further studies.

CONCLUSIONS

Taken together, these data indicate a pivotal role of miR-132 in the mediation of pathologic hypertrophy of the heart. Moreover, they indicate an efficient treatment option to prevent the conversion of physiologic to pathologic hypertrophy by miR-132 inhibition, and thereby expanding the potential of antimiR-132 treatment in patients with heart failure of nonischemic origin. Clinical studies extending the first-in-man application in patients with heart failure (12) by efficacy studies in various patients with heart failure will address the potential of this novel therapeutic concept.

ACKNOWLEDGMENT The authors thank Anja Wolf for expert technical assistance.

FUNDING SUPPORT AND AUTHOR DISCLOSURES

This study was supported by the Deutsches Zentrum für Herz-Kreislauf-Forschung (German Centre for Cardiovascular Research) (to Drs. Hinkel, Weber, Engelhardt, Laugwitz, Moretti, and Kupatt) and, with regard to model development, by the Deutsche Forschungsgemeinschaft (German Research Foundation) (TRR 267 to Drs. Thum, Weber, Engelhardt, Laugwitz, and Kupatt.; and KFO311 to Dr. Thum.). Drs. Baktai and Thum are founders of Cardior Pharmaceuticals GmbH and hold shares. Dr. Thum filed and licensed patents in the field of noncoding ribonucleic acids including miR-132. All other authors have reported that they have no relationships relevant to the contents of this paper to disclose.

ADDRESS FOR CORRESPONDENCE: Dr. Christian Kupatt, Klinik und Poliklinik für Innere Medizin I, University Clinic rechts der Isar, Technical University Munich, Ismaninger Strasse 22, 81675 Munich, Germany. E-mail: Christian.kupatt@tum.de. OR Dr. Thomas Thum, Institute of Molecular and Translational Therapeutic Strategies, Hannover Medical School, Carl-Neuberg-Strasse 1, 30625 Hannover, Germany. E-mail: thum.thomas@mh-hannover.de. Twitter: @Rabea08515954.

PERSPECTIVES

COMPETENCY IN MEDICAL KNOWLEDGE: Intracoronary injection of an antimiR-132 reduces cardiomyocyte cross-sectional area, retards fibrosis, and improves capillary density and LV ejection fraction in a pig model of myocardial hypertrophy.

TRANSLATIONAL OUTLOOK: Randomized clinical trials are needed to evaluate the safety and efficacy of antimiR-132 in patients with hypertrophic cardiomyopathy.

REFERENCES

1. Marian AJ, Braunwald E. Hypertrophic cardiomyopathy: genetics, pathogenesis, clinical manifestations, diagnosis, and therapy. Circ Res 2017;121:749–70.

2. Yamanaka S, Sakata Y, Nochioka K, et al., for the CHART-2 Investigators. Prognostic impacts of dynamic cardiac structural changes in heart failure patients with preserved left ventricular ejection fraction. Eur J Heart Fail 2020;22:2258–68.

3. Lip GYH, Coca A, Kahan T, et al. Hypertension and cardiac arrhythmias: executive summary of a consensus document from the European Heart Rhythm Association (EHRA) and ESC Council on Hypertension, endorsed by the Heart Rhythm Society (HRS), Asia-Pacific Heart Rhythm Society (APHRS), and Sociedad Latinoamericana de Estimulación Cardíaca y Electrofisiología (SOLEACE). Eur Heart J Cardiovasc Pharmacother 2017;3:235–50.

4. Camici PG, Tschöpe C, Di Carli MF, Rimoldi O, Van Linthout S. Coronary microvascular dysfunction in hypertrophy and heart failure. Cardiovasc Res 2020;116:806–16.

5. Shimizu I, Minamino T. Physiological and pathological cardiac hypertrophy. J Mol Cell Cardiol 2016;97:245–62.

6. Ponikowski P, Voors AA, Anker SD, et al. 2016 ESC guidelines for the diagnosis and treatment of acute and chronic heart failure: the task Force for the diagnosis and treatment of acute and chronic heart failure of the European Society of Cardiology (ESC). Developed with the special contribution of the Heart Failure Association (HFA) of the ESC. Eur Heart J 2016;37:2129–200.

7. Shiojima I, Sato K, Izumiya Y, et al. Disruption of coordinated cardiac hypertrophy and angiogenesis contributes to the transition to heart failure. J Clin Invest 2005;115:2108–18.

8. Franssen C, Chen S, Unger A, et al. Myocardial microvascular inflammatory endothelial activation in heart failure with preserved ejection fraction. J Am Coll Cardiol HF 2016;4:312–24.

9. Ucar A, Gupta SK, Fiedler J, et al. The miRNA-212/132 family regulates both cardiac hypertrophy and cardiomyocyte autophagy. Nat Commun 2012;3:1078.

10. Foinquinos A, Batkai S, Genschel C, et al. Preclinical development of a miR-132 inhibitor for heart failure treatment. Nat Commun 2020;11:633.

11. Batkai S, Genschel C, Viereck J, et al. CDR132L improves systolic and diastolic function in a large animal model of chronic heart failure. Eur Heart J 2021;42:192–201.

12. Täubel J, Hauke W, Rump S, et al. Novel antisense therapy targeting microRNA-132 in patients with heart failure: results of a first-in-human phase 1b randomized, double-blind, placebo-controlled study. Eur Heart J 2021;42:178–88.

13. Kumarswamy R, Volkmann I, Beermann J, et al. Vascular importance of the miR-212/132 cluster. Eur Heart J 2014;35:3224–31.

14. Eskildsen TV, Jeppesen PL, Schneider M, et al. Angiotensin II regulates microRNA-132/-212 in hypertensive rats and humans. Int J Mol Sci 2013;14:11190–207.

15. Cheng X, Ku C-H, Siow RCM. Regulation of the Nrf2 antioxidant pathway by microRNAs: new players in micromanaging redox homeostasis. Free Radic Biol Med 2013;64:4–11.

16. Hinkel R, Ramanujam D, Kaczmarek V, et al. AntimiR-21 prevents myocardial dysfunction in a pig model of ischemia/reperfusion injury. J Am Coll Cardiol 2020;75:1788–800.

17. Ucar A, Vafaizadeh V, Jarry H, et al. miR-212 and miR-132 are required for epithelial stromal interactions necessary for mouse mammary gland development. Nat Genet 2010;42:1101–8.

18. Zhou Y, Li KS, Liu L, Li SL. MicroRNA-132 promotes oxidative stress-induced pyroptosis by targeting sirtuin 1 in myocardial ischaemia-reperfusion injury. Int J Mol Med 2020;45:1942–50.

19. Tirziu D, Chorianopoulos E, Moodie KL, et al. Myocardial hypertrophy in the absence of external stimuli is induced by angiogenesis in mice. J Clin Invest 2007;117:3188–97.

20. Gogiraju R, Bochenek ML, Schäfer K. Angiogenic endothelial cell signaling in cardiac hypertrophy and heart failure. Front Cardiovasc Med 2019;6:20.

21. Captur G, Heywood WE, Coats C, et al. Identification of a multiplex biomarker panel for hypertrophic cardiomyopathy using quantitative proteomics and machine learning. Mol Cell Proteomics 2020;19:114–27.

22. Sager HB, Hulsmans M, Lavine KJ, et al. Proliferation and recruitment contribute to myocardial macrophage expansion in chronic heart failure. Circ Res 2016;119:853–64.

23. Wang L, Zhang YL, Lin QY, et al. CXCL1-CXCR2 axis mediates angiotensin II-induced cardiac hypertrophy and remodelling through regulation of monocyte infiltration. Eur Heart J 2018;39:1818–31.

24. Shimada S, Abais-Battad JM, Alsheikh AJ, et al. Renal perfusion pressure determines infiltration of leukocytes in the kidney of rats with angiotensin II-induced hypertension. Hypertension 2020;76:849–58.

25. Hinkel R, Hoewe A, Renner S, et al. Diabetes mellitus-induced microvascular destabilization in the myocardium. J Am Coll Cardiol 2017;69:131–43.

26. Maejima Y, Kuroda J, Matsushima S, Ago T, Sadoshima J. Regulation of myocardial growth and death by NADPH oxidase. J Mol Cell Cardiol 2011;50:408–16.

27. Panera N, Gnani D, Piermarini E, et al. High concentrations of H2O2 trigger hypertrophic cascade and phosphatase and tensin homologue (PTEN) glutathionylation in H9c2 cardiomyocytes. Exp Mol Pathol 2016;100:199–206.

28. Li J, Ichikawa T, Villacorta L, et al. Nrf2 protects against maladaptive cardiac responses to hemodynamic stress. Arterioscler Thromb Vasc Biol 2009;29:1843–50.

29. Potente M, Ghaeni L, Baldessari D, et al. SIRT1 controls endothelial angiogenic functions during vascular growth. Genes Dev 2007;21:2644–58.

30. Ziegler T, Horstkotte J, Schwab C, et al. Angiopoietin 2 mediates microvascular and hemodynamic alterations in sepsis. J Clin Invest 2013;123:3436–45.

31. Hellstrom M, Kalen M, Lindahl P, Abramsson A, Betsholtz C. Role of PDGF-B and PDGFR-beta in recruitment of vascular smooth muscle cells and pericytes during embryonic blood vessel formation in the mouse. Development 1999;126:3047–55.

KEY WORDS adverse cardiac remodeling, antimiR-132, cardiac hypertrophy, heart failure, microRNA-132

APPENDIX For supplemental figures, please see the online version of this paper.